Applied Catalysis B: Environmental 217 (2017) 57–64

Contents lists available at ScienceDirect

Applied Catalysis B: Environmental

journal homepage: www.elsevier.com/locate/apcatb

Compact and uniform TiO_2@g-C_3N_4 core-shell quantum heterojunction for photocatalytic degradation of tetracycline antibiotics

Wei Wang[a,b,*], Jiaojiao Fang[b], Shaofeng Shao[a], Min Lai[a], Chunhua Lu[b]

[a] Jiangsu Key Laboratory for Optoelectronic Detection of Atmosphere and Ocean, School of Physics and Optoelectronic Engineering, Nanjing University of Information Science & Technology, Nanjing 210044, China
[b] Jiangsu Collaborative Innovation Center for Advanced Inorganic Function Composites, Nanjing Tech University, Nanjing 210009, China

ARTICLE INFO

Article history:
Received 21 February 2017
Received in revised form 2 May 2017
Accepted 11 May 2017
Available online 11 May 2017

Keywords:
g-C_3N_4 quantum shell
{001} TiO_2
Surface heterojunction
Tetracycline degradation
Photocatalysis

ABSTRACT

Optimizing the heterojunction structure of semiconductor photocatalysts is significant for taking full advantage of their abilities for organic molecules degradation. Here, we demonstrate a feasible strategy of polymerizing the quantum-thick graphitic carbon nitride (g-C_3N_4) on to the surface of anatase titanium dioxide (TiO_2) nanosheets with exposed {001} facets to form the TiO_2@g-C_3N_4 (TCN) core-shell quantum heterojunction for improving photocatalytic tetracycline degradation activity. 100 mg of TCN photocatalyst shows the highest tetracycline degradation rate of 2.2 mg/min, which is 36% higher than that of the TiO_2/g-C_3N_4 random mixture (TCN(mix)), 2 times higher than that of TiO_2, and 2.3 times higher than that of bulk g-C_3N_4. Results also indicate that h^+ and $\cdot O_2^-$ are the main oxidant species for the efficient photocatalytic reaction. The decisive factors in improving the photocatalytic activity of TCN is the unique structural advantages of quantum-thick g-C_3N_4 shell, compact and uniform contact interface, richly available reaction sites, more surface adsorbed hydroxyl (OH) groups. Efficient electron transfer between TiO_2 and g-C_3N_4 is also demonstrated by the significant enhancement of photocurrent response of TCN electrodes and decrement of fluorescence emission spectra. This work demonstrates new sights for synthesizing high-efficient and environment-stable photocatalysts by engineering the surface heterojunction.

1. Introduction

Photocatalysis is an efficient technology in decomposing organic water pollutant molecules, such as dyes and antibiotics [1–3]. High activity and stability are key factors in affecting the practical application of semiconductor photocatalysts [4,5]. Anatase TiO_2 nanosheet with exposed {001} and {101} facets is one of the most promising semiconductor photocatalyst to deal with the environmental pollution due to its well balance among environmental stability, non-toxic, low cost, and UV-driven high activity [6]. Various effects have been devoting to modifying such TiO_2 with quantum dots, noble metals, graphene etc. to improve the light absorption, photo-generated carriers' separation, and reactants' adsorption [7–9]. Compositing TiO_2 with narrow bandgap semiconductors to form heterojunction is also an efficient strategy for achieving these goals. From the aspect of "Green Material", the metal-free, stable, and visible-light responsive g-C_3N_4 is a promising candidate to composite with TiO_2 to form efficient heterojunction for photocatalytic application [10].

G-C_3N_4, constituted by numerous layers of two-dimensional (2D) counterparts, can be prepared by ploycondensation of organic precursors such as urea, cyanamide, dicyandiamide, and thioruea [11–13]. Studies have confirmed that g-C_3N_4 is an efficient candidate for efficient photocatalytic waste water treatment, CO_2 reduction, and H_2 production [14–16]. The obtained bulk g-C_3N_4 often possesses a low specific surface area, irregular morphology, and a hydrophobic surface, restricting its photocatalytic application. To increase the photocatalytic activity, introducing nitrogen vacancy, heteroatoms, and other function materials are widely employed [17–20]. For instance, Cu(II) meso-Tetra (4-carboxyphenyl) porphyrin sensitized g-C_3N_4 can significantly enhance photocatalytic phenol degradation due to both improved electron transfer efficiency and visible light absorption efficiency

* Corresponding author at: Jiangsu Key Laboratory for Optoelectronic Detection of Atmosphere and Ocean, School of Physics and Optoelectronic Engineering, Nanjing University of Information Science & Technology, Nanjing 210044, China.
E-mail address: wwang@nuist.edu.cn (W. Wang).

http://dx.doi.org/10.1016/j.apcatb.2017.05.037
0926-3373/

[21]. Employing zeolitic imidazolate frameworks or metal-organic frameworks, which has a high specific surface area, to hybrid g-C_3N_4 can significantly improve the efficiencies toward target molecules adsorption and decomposition [15,22,23]. Studies also show that reducing the thickness of bulk g-C_3N_4 is also benefit for improving the photocatalytic activity, which is due to the higher specific surface area, more exposed active sites, and easier transfer the photo-generated carriers to the outer surface [24–26]. Three strategies are commonly employed to exfoliate the bulk g-C_3N_4 to the fewer-layered counterparts [27,28]. Firstly, liquid exfoliation is the most widely employed strategy. It's reported that the theoretical Van der Waals force between the neighboring g-C_3N_4 layers is ca. 70 mJ/m^2 [28]. This value is reported of ca. 115 mJ/m^2 in the work by Zhang et al. [29]. As a result, both water and isopropanol are considered as efficient agents to insert into the g-C_3N_4 layer spaces so as to exfoliate them to thin nanosheets by employing ultrasonic method or high-energy shear method. The second strategy is thermal oxidation etching. Niu and Cheng et al. successfully prepared g-C_3N_4 nanosheets by simply annealing bulk g-C_3N_4 in the air atmosphere at 500 °C. The thickness of g-C_3N_4 can be reduced by prolonging the thermal etching time [30]. The third strategy is solvothermal exfoliation. Han et al. successfully synthesized atomically thin mesoporous g-C_3N_4 nanomesh by combining the solvothermal exfoliation process with the liquid exfoliation process [24]. Based on the above methods, the obtained fewer-layered g-C_3N_4 sheets are high-reactive and can be applied widely to solve environmental contamination and energy crisis problems. However, both the methods have complicate exfoliation processes and low productivity (often less than 10%). To proceed the large-scale application, more facial and efficient method is needed.

Physical blend and unordered sintering are the commonly employed methods to prepare g-C_3N_4/TiO_2 composites. Most works are focusing on finding out an optimum ratio between g-C_3N_4 and TiO_2 so as to get the highest photocatalytic activity [31,32]. As is well known, compact and efficient contact between each part is significant for facilitating the electrons' transfer at the interface. Even the g-C_3N_4 sheets are superior than bulk g-C_3N_4 to form heterojunction with TiO_2 by the physical mixing method due to the high specific surface area and the flexible 2D structure, the resulted contact between TiO_2 and g-C_3N_4 is loose and non-uniform. Then chemical bonding method is widely considered to be more favorable than physical mixing to form compact and uniform contact interfaces. More detailed works focusing on optimizing the surface heterojunction structure may give new insights on improving the photocatalytic activity of TiO_2/g-C_3N_4 composites.

Herein, by utilizing urea and {001}-faceted TiO_2 as precursors, we developed a simple strategy to in situ synthesize a high-reactive photocatalyst with compact and uniform TiO_2@g-C_3N_4 core-shell quantum heterojunction. Compared to the random composite of TiO_2 and g-C_3N_4, the new photocatalyst dramatically optimize the physicochemical properties and enhance the photocatalytic activity for tetracycline degradation under xenon lamp irradiation.

2. Experimental

2.1. Preparation of photocatalysts

Bulk g-C_3N_4 was prepared by annealing 10 g urea in a covered crucible (20 mL) at 520 °C for 2 h with a ramping speed of 5 °C/min. TiO_2 nanosheets with exposed {001} facets were prepared according to our previous procedure [33]. After that, 1 g TiO_2 and 10 g urea were simply mixed together by ball-milling, following by transferring to the covered crucible. The random mixture of g-C_3N_4 and TiO_2 (TCN(mix)) was synthesized by annealing the precursor at 520 °C for 2 h in the N_2 atmosphere. In order to prepare TiO_2@g-C_3N_4 core-shell quantum heterojunction (TCN), 10 g urea was dissolved in 10 mL deionized water, followed by the addition of 1 g TiO_2. The homogeneous suspension was centrifuged after magnetic stirring for 1 h in a vacuum system, followed by drying thoroughly in a vacuum oven at 60 °C. Even most of the urea was washed away by the deionized water during the centrifugation process, a small portion of urea adsorbed on the TiO_2 surface is still left. Then the solid block without grinding was wrapped with 3 layers of aluminum foil, followed by annealing at 520 °C for 2 h in the N_2 atmosphere with a ramping speed of 5 °C/min. During the heat treatment process, the aggregated mixture and the tightly wrapped aluminum foil helps to restrict the polymerization space of g-C_3N_4. As a result, the g-C_3N_4 quantum shell can be in situ synthesized on the TiO_2 surface. Finally, TCN was grinded to obtain the powder photocatalyst.

2.2. Characterization

X-ray diffraction (XRD) spectra were obtained using an X-ray diffractometer (SmartLab-3KW, Rigaku) with a Cu Kα irradiation source at a scanning speed of 10°/min. X-ray photoelectron spectroscopy (XPS) analysis was conducted on a PHI5000 Versaprobe system with monochromatic Al Kα radiation. Light absorption analysis was conducted on a UV-vis-NIR spectrometer (UV-3010, Shimadzu). Fluorescence emission analysis was conducted on a fluorescence spectrophotometer (FL3-221, Jobin Yvon) at room temperature. Brunauer-Emmett-Teller (BET) specific surface area was obtained by nitrogen adsorption-desorption isotherm analysis. The morphology of the photocatalysts was analyzed by scanning (SEM, Hitachi S4800) and transmission (TEM, JEOL 2100) electron microscopy. Fourier Transformed Infrared (FTIR) spectra were analyzed on a Vector-22 spectrometer. TG analysis was conducted on a thermos gravimetric analyzer (Q500, TA) with temperature increased from room temperature to 800 °C in the air atmosphere.

2.3. Photoelectrochemical measurements

The photoelectrode was prepared by employing the glassy carbon electrode with an exposed diameter of 3 mm [34]. A homogeneous suspension was prepared by dispersing 20 mg photocatalyst in the solution containing 1 mL ethanol and 10 μL naphthol. Then 20 μL of the suspension was dip-coated on the glassy carbon electrode, followed by drying in a vacuum oven at 60 °C for 24 h. Photocurrent measurements were conducted on a Chenhua CHI660E electrochemical analyzer using a standard three-electrode system with a Pt counter electode, a Ag/AgCl reference electrode, and the glassy carbon working electrode. A 0.2 M Na_2SO_4 aqueous solution was used as the electrolyte. The i-t curve was measured at 0 V bias potential under a 300 W xenon lamp full spectrum (Beijing PerfecLight Technology Co., Ltd.) irradiation.

2.4. Photocatalytic measurements

Photocatalytic tetracycline degradation was carried out in a top-irradiation vessel connected to a circulating cooling system. A total of 100 mg of as-prepared photocatalyst was dispersed in 100 mL of tetracycline aqueous solution (20 mg/L). The xenon lamp with full spectrum irradiation was employed as the light source to drive the photocatalytic reaction. The temperature was maintained below 25 °C during the photocatalytic experiment process. At certain time intervals, 3 mL of the suspension was collected to remove the photocatalyst by centrifugation. The photocatalytic degradation efficiency of tetracycline was analyzed on the UV-vis-NIR spectrophotometer by recording the absorption spectrum of the aqueous solution. In order to investigate the main oxidant species of the photocatalytic reaction, isopropanol (IPA), ethylenediaminete-

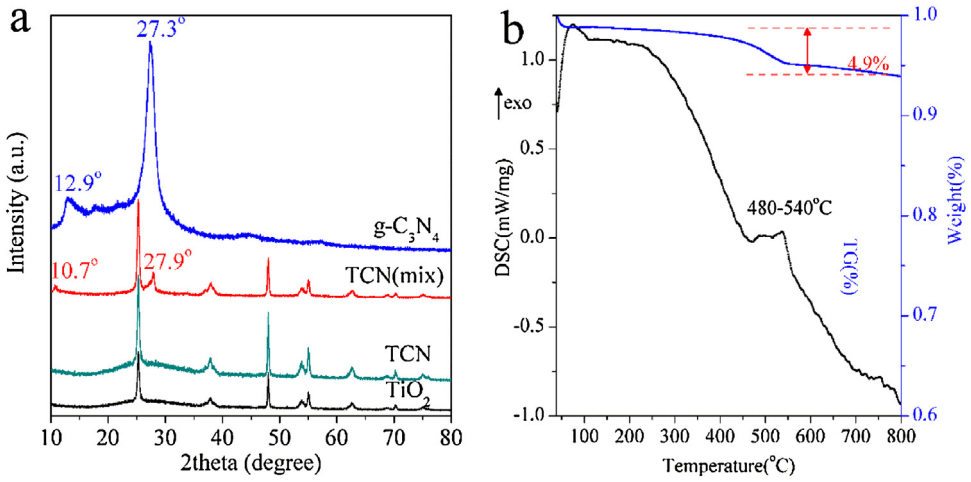

Fig. 1. (a) XRD patterns of TiO_2, g-C_3N_4, TCN(mix), and TCN. (b) TG and DSC curves of TCN analyzed in the air atmosphere.

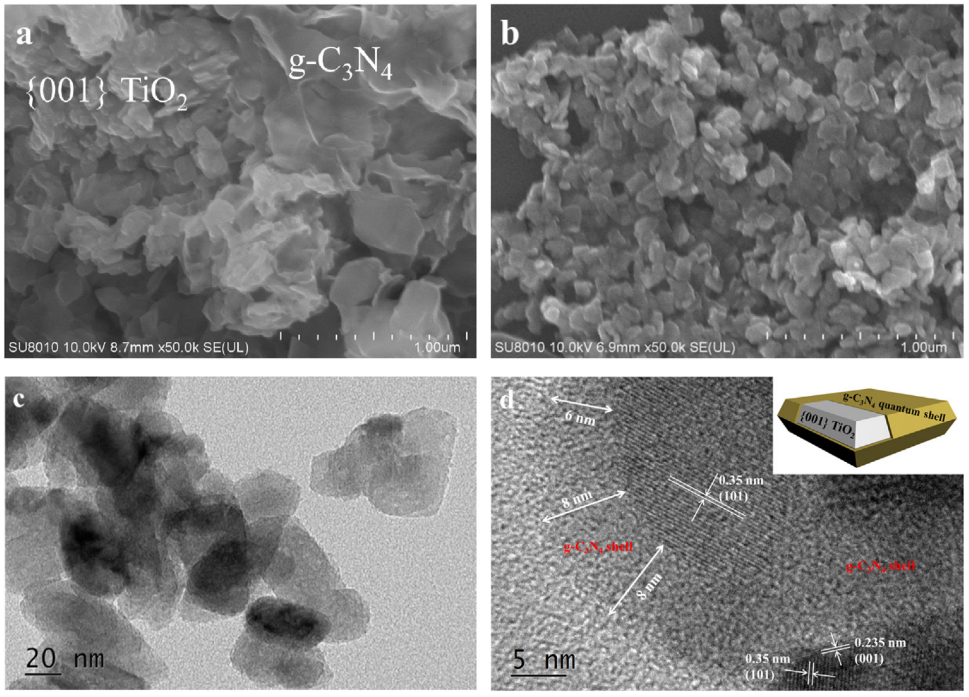

Fig. 2. SEM and TEM images of (a) TCN(mix) and (b,c,d) TCN.

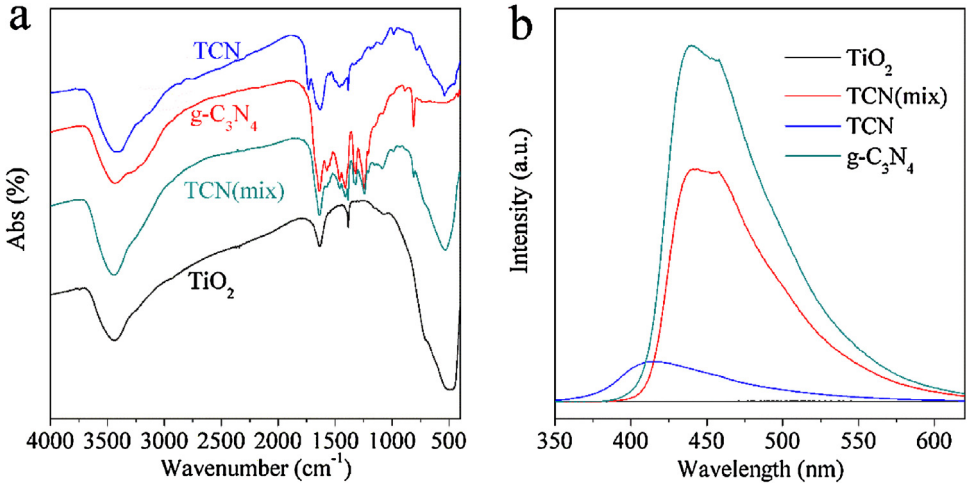

Fig. 3. (a) FTIR and (b) fluorescence emission spectra (λ_{ex} = 300 nm) of TiO_2, TCN, TCN(mix), and g-C_3N_4.

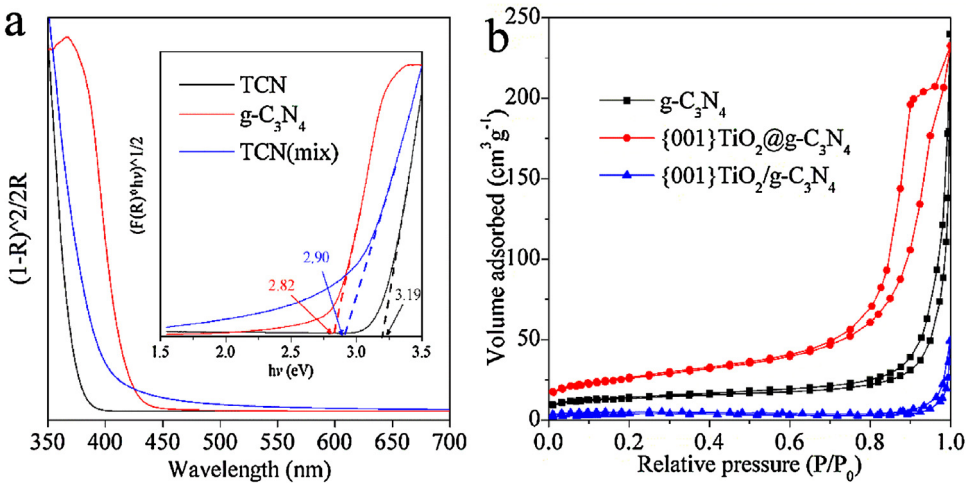

Fig. 4. (a) Light absorption spectra and estimated band gaps (inset), and (b) N_2 adsorption-desorption isotherms of TCN, TCN(mix), and g-C_3N_4.

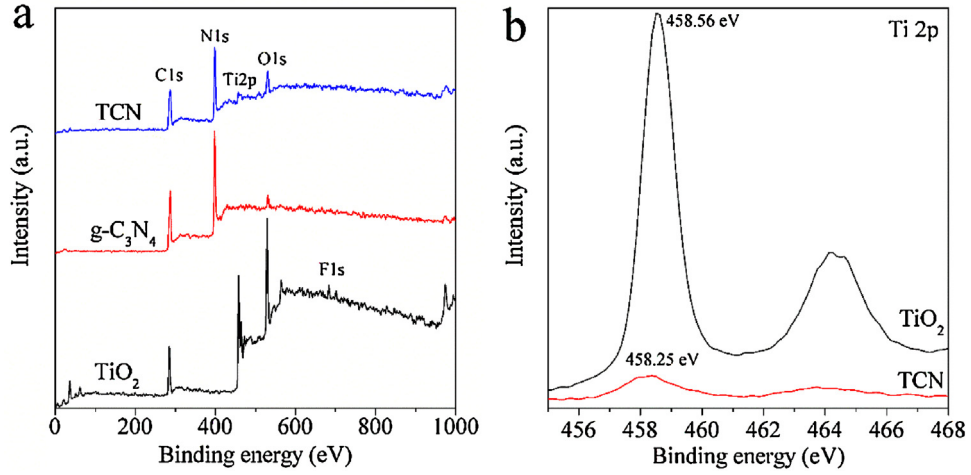

Fig. 5. (a) Survey XPS spectra and (b) high-resolution Ti 2p XPS spectra of TiO_2, TCN, and g-C_3N_4.

traacetic acid disodium salt (EDTA), and benzoquinone (BQ) were employed as the scavengers for ·OH, h^+, and $\cdot O_2^-$, respectively. The dosages of all sacrificial agent are 0.01 M [35].

3. Results and discussion

XRD patterns are firstly used to reveal phase compositions of the photocatalysts (Fig. 1a). The bulk g-C_3N_4 gives typical diffraction peaks centered at 27.3° and 12.9° stemmed from periodic stacking of 2D layers and in-plane ordering of tri-*s*-triazine unites, respectively [10,24]. Similar diffraction peaks with much lower intensity are also observed for TCN(mix), indicating the g-C_3N_4 is also synthesized with the presence of TiO_2. Close observation indicates both the diffraction peaks shift to 27.9° and 10.7°, respectively, suggesting the g-C_3N_4 in TCN(mix) has a smaller inter-planar stacking distance, a larger distance and more short-range order of in-planar structure packing [24,36]. These features could be explained by that the presence of TiO_2 favors to influence the polymerization process of g-C_3N_4, and then rearrange its structure. In contrast, no diffraction peaks ascribed to g-C_3N_4 are observed in TCN. During the preparation process of TCN, the lower-content urea is dispersed uniformly in the TiO_2/ureaprecursor. Thus a much lower content and more uniform dispersion of g-C_3N_4 in TCN is possible. The TG and DSC analysis of TCN are conducted to investigate its g-C_3N_4 content (Fig. 1b). As is well-known, the strong Van der Waals' force among the g-C_3N_4 layers can be destroyed by heat treatment in the air atmosphere. Thus the weight loss at a temperature lower than 480 °C is ascribed to the continuous evaporation of g-C_3N_4 because of the weakened Van der Waals' force. Moreover, the DSC curve shows an exothermal peak, which is due to the decomposition of g-C_3N_4, in the temperature interval between 480 °C and 540 °C. Regardless of the moisture loss at ca. 100 °C, the content of g-C_3N_4 in TCN is ca. 4.9%. Moreover, the anatase phase of TiO_2 is well-maintained and the crystallinity is improved after the heat treatment. The (101) diffraction peak of both TCN and TCN(mix) has not been shifted, suggesting no impurity atoms or oxygen vacancies are introduced into the TiO_2 matrix (Fig. S1) [37].

The as-prepared TiO_2 has clearly distinguished {001} and {101} facets (Fig. S2a,b) [33]. The smooth surface of TiO_2 is well maintained after annealed at 520 °C in the N_2 atmosphere, but the sheet structure is slightly changed (Fig. S2c). SEM image of TCN(mix) shows that TiO_2 and g-C_3N_4 are randomly aggregated with each other (Fig. 2a). The g-C_3N_4 seems to serve as the binder among the TiO_2 nanosheets, suggesting the TiO_2 can truly change the morphology of g-C_3N_4 (Fig. S2d). This non-uniform dispersion is completely changed in TCN which shows no obvious g-C_3N_4 on the TiO_2 surface in the SEM image (Fig. 2b). The TEM observation indicates that TCN has a rough surface (Fig. 2c), which is different from that of the annealed TiO_2. Moreover, the (101) and (001) lattice spacing of 0.35 nm and 0.235 nm, respectively, ascribed to TiO_2 can be defined

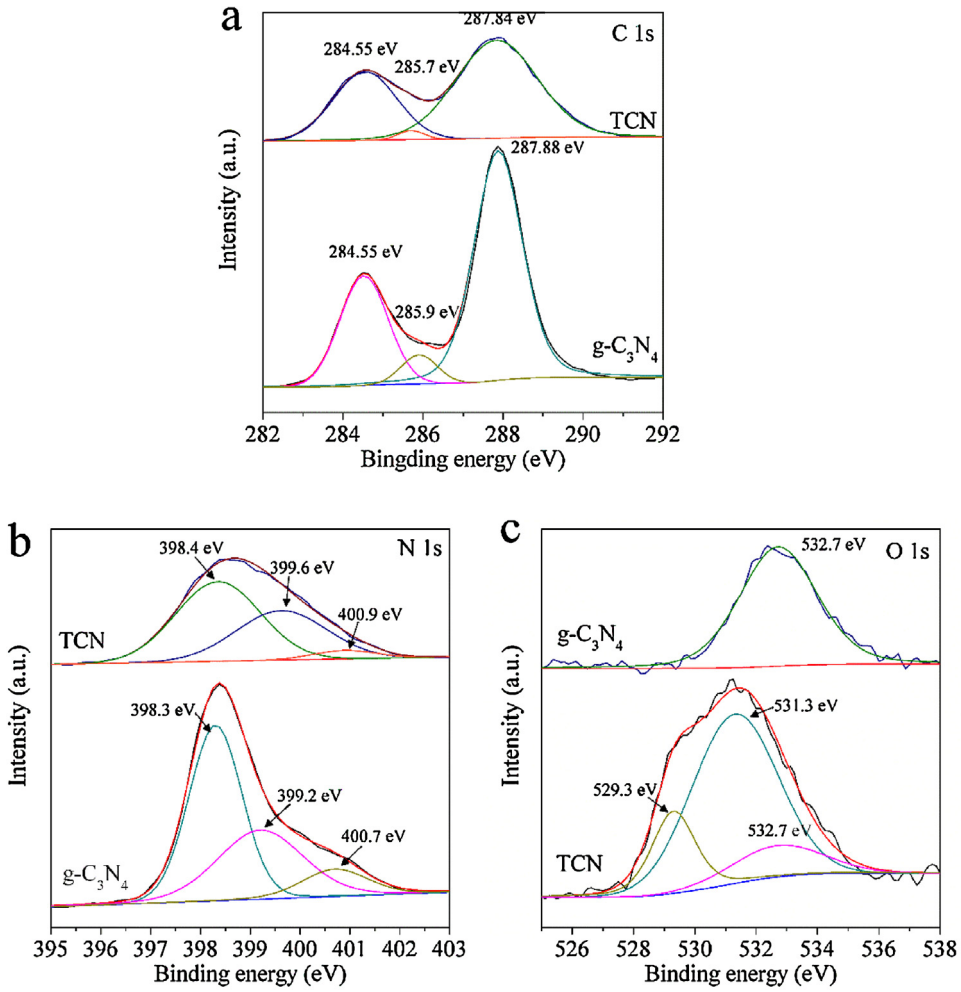

Fig. 6. High-resolution (a) C1s, (b) N 1s, and (c) O 1 s XPS spectra of TCN and g-C_3N_4.

clearly in TCN (Fig. 2d). Obviously, the TiO_2 is covered with a layer of amorphous g-C_3N_4 with a thickness of ca. 6–8 nm. Such structured g-C_3N_4 will give an intense quantum confinement effect and may benefit the photocatalytic reaction [26]. This contact interface is also more compact and uniform than that of TCN(mix).

The formation of g-C_3N_4 quantum shell on TiO_2 can be further proved by the FTIR analysis (Fig. 3a). The bands at ca. 3045 cm^{-1} corresponds to the surface-bonded OH groups. Another wide band originated from N—H vibration appears in the range of ca. 3015–3252 cm^{-1} of g-C_3N_4, TCN, and TCN(mix). TiO_2 shows the strongest characteristic Ti-O-Ti stretching vibration peak at ca. 520 cm^{-1}. This peak of TCN is much weaker than that of TCN(mix), indicating the TiO_2 nanosheets of TCN is fully covered with the g-C_3N_4 quantum shell. In contrast, many TiO_2 nanosheets of TCN(mix) are exposed because of the inhomogeneous TiO_2-urea precursor. The sharp peak at ca. 784 cm^{-1} belongs to the heptazine ring [24]. Compared to g-C_3N_4, lower intensity of this peak suggests the less ordered in-plane structural packing motif in both TCN and TCN(mix). Several strong bands in the region of ca. 1200–1650 cm^{-1} corresponding to the typical stretching mode of CN heterocycles can also be observed for g-C_3N_4 and TCN(mix). However, these peaks show obvious red-shift for TCN, which may because of the strong interaction between TiO_2 and the g-C_3N_4 quantum shell. This close and intense interaction may facilitate the photo-carriers' transfer at the TiO_2/g-C_3N_4 interface.

The different g-C_3N_4 structure among these photocatalysts can also be confirmed by the fluorescence emission spectra (Fig. 3b). Compared to the weak fluorescence emission spectrum of TiO_2, g-C_3N_4 shows a strong and wide emission peak due to its fast recombination of photo-generated electrons and holes [38,39]. Notably, a similar fluorescence emission peak is also observed in TCN(mix), suggesting the well-maintained g-C_3N_4 structure. The observed lower intensity allows us to get the positive effect of the non-uniform TiO_2/g-C_3N_4 heterojunction. Importantly, the much lower fluorescence emission peak of TCN shows an obvious blue-shift, which should be attributed to the quantum confinement effect of g-C_3N_4 quantum shell [40,41] and its more intense contact with TiO_2.

The band gaps of TCN and TCN(mix) are further studied by the light absorption spectra. The absorption edges of both TCN(mix) and TCN show blue shift comparing to that of bulk g-C_3N_4 (Fig. 4a). The estimated band gaps of bulk g-C_3N_4, TCN(mix), and TCN are 2.82 eV, 2.90 eV, and 3.19 eV (inset in Fig. 4a). It's obvious that the g-C_3N_4 with reduced layers in TCN(mix) and TCN introduce strong quantum confinement effect which significantly widen the band gap [12,26]. BET analysis shows the specific surface area of as-prepared g-C_3N_4 is 33.12 m^2/g, while the specific surface area of TCN(mix) is only 15.18 m^2/g (Fig. 4b). This result is consistent with the SEM analysis which indicates the g-C_3N_4 is mainly served as the binder among the TiO_2 nanosheets. In contrast, TCN gets the highest specific surface area (51.87 m^2/g) because of its good monodispersity. In this respect, the TCN may expose more reaction sites for photocatalytic tetracycline degradation.

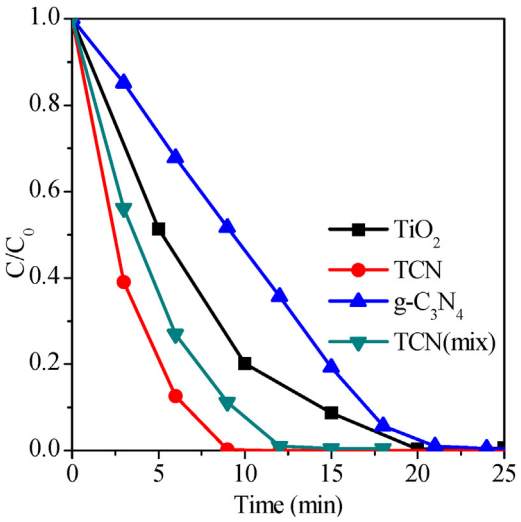

Fig. 7. Photocatalytic degradation efficiencies of tetracycline by employing TiO_2, TCN, TCN(mix), and g-C_3N_4 as the photocatalysts under the xenon lamp irradiation.

XPS analysis is carried out to determine the special chemical state of TCN. It's observed that both TCN and pure g-C_3N_4 are rich in C and N elements (Fig. 5a). Compared to TiO_2, a weak signal ascribed to Ti is also detected in TCN due to the shielding effect of g-C_3N_4 quantum shell. The Ti 2p signal of TCN shows a clear blue-shift because of the intense interface interaction (Fig. 5b). Then the surface chemical environment of g-C_3N_4 quantum shell is different from that of pure g-C_3N_4. The g-C_3N_4 C 1 s spectrum shows three main peaks, which should be assigned to adventitious carbon species (284.55 eV), C-$(N)_3$ species (285.9 eV), and C—N—C (287.88 eV) (Fig. 6a) [36,42]. Notably, the latter two peaks of TCN have a relative lower binding energy. In contrast, the N 1 s spectrum of TCN shows a red-shift compared to that of pure g-C_3N_4 (Fig. 6b). The three peaks of N 1 s could be assigned to C—N═C (398.5 eV), N-$(C)_3$ (399.8 eV), and C—NH (401.0 eV). Importantly, the intensity ratio of (C—N═C)/(N-$(C)_3$) decreases from 2.52 to 1.39 and the C/N atomic ratio increases from 0.752 to 0.758, indicating some of the N atoms has been replaced by other atoms in TCN [36]. The O 1 s spectrum of pure g-C_3N_4 shows only one peak centered at 532.7 eV, which could be assigned to the adsorbed H_2O molecules (Fig. 6c). However, the TCN O 1 s spectrum also suggests its surface is rich in OH groups (531.3 eV). The peak at 529.3 eV is originated from the inner Ti-O-Ti bond, which is similar to that of TiO_2 (Fig. S3). Thus it could be assumed that some N atoms of g-C_3N_4 quantum shell should have been replaced by the O atoms. The above signal variations between pure g-C_3N_4 and TCN should be originated from their different layer structures and the intense interaction between g-C_3N_4 quantum shell and TiO_2. The OH groups adsorbed on TCN surface will help it to contact with the hydrophilic tetracycline molecules and facilitate the photocatalytic reaction.

TCN shows the highest activity in the photocatalytic degradation of tetracycline because of its superior structure (Fig. 7). 100 mg TCN can decompose 2 mg tetracycline in 9 min (2.2 mg/min), which is 36% faster than that of TCN(mix), 2.3 times faster than that of pure g-C_3N_4, and 2 times faster than that of TiO_2. It's widely accepted that TiO_2/g-C_3N_4 heterojunction is positive for separating the photo-generated electrons and holes. However, the TiO_2/g-C_3N_4 heterojunction formed by random mixing is loose and non-uniform, which also reduces the surface area (Fig. 8a). As shown in Table S1, various photocatalysts prepared by annealing the urea/TiO_2 random mixtures with different weight ratios were also employed to degrade tetracycline. Comparing to TCN(mix), all the photocatalysts show lower activities in the degradation of tetracycline. At a lower urea content, the as-synthesized g-C_3N_4 can't warp tightly and uniformly on the TiO_2 surface, reducing the positive effect of the surface heterojunction. In contrast, a higher urea content will result in too much g-C_3N_4 wrapped on the TiO_2 surface in the final samples, reducing the excitation efficiency of TiO_2 and the photocatalytic activity. Both factors were well balanced for TCN(mix) prepared with weight ratio of urea to TiO_2 is 10. In contrast, the TCN has a compact and uniform g-C_3N_4 quantum shell. This structure not only facilitates the photo carriers' separation, but also absorbs more surface OH groups and keeps the high specific surface area. The reduced thickness and improved quantum confinement effect of g-C_3N_4 quantum shell also give TCN a higher photocatalytic activity. The much higher photocatalytic activity of TCN further confirms the significance of tight and uniform contact by surface heterojunction engineering. The positive structure of TCN can also be revealed in the photocurrent analysis (Fig. 8b). A higher photocurrent density often means a higher ability in separating the photo-generated electrons and holes. Because of the compact and uniform contact between TiO_2 and g-C_3N_4 quantum shell, TCN presents the highest photocurrent density. In this view, the loose and non-uniform contact in TCN(mix) will surely reduce the photocurrent density and the photocatalytic activity. Moreover, all the photocatalysts show a stable ability in separating the photo-generated electrons and holes. Thus the photocatalytic activity of TCN is almost unchanged after 4 cyclic reactions (Fig. S4). The crystal phase and TEM image of the used TCN were analyzed to confirm its stability (Fig. 9a). The anatase phase of TiO_2 was well maintained after four cycles of photocatalytic reaction. No diffraction peaks ascribed to g-C_3N_4 was observed, suggesting its mono-dispersion on the TiO_2 surface. TEM image (Fig. 9a, inset) clearly shows the g-C_3N_4 quantum shell covered on the TiO_2 surface has a thickness of ca. 6 nm, convincing the structural stability of TCNGenerally, excitation of TCN will cause the formation of h^+, ·OH, and $\cdot O_2^-$, which are considered to be the possible active oxidant species to degrade organic molecules (Eqs. (1)–(4)). IPA, BQ, and EDTA were employed as the scavengers for ·OH, $\cdot O_2^-$, and h^+, respectively. As shown in Fig. 9b, there is little change of the tetracycline degradation efficiency when IPA is added into the reaction system, while that efficiency is significantly reduced with the addition of BQ and EDTA. The band potential of semiconductor photocatalyst can be determined by the empirical equation [43]:

$$E_{VB} = \chi - E^e + 0{\cdot}5E_g$$

$$E_{CB} = E_{VB} - E_g$$

Where E^e (ca. 4.5 eV) is the energy of free electrons with the hydrogen scale. The χ, which is the absolute electronegativity of the semiconductor, values for TiO_2 and g-C_3N_4 are 5.86 eV and 4.73 eV, respectively. In the present study, the band gap of the quantum g-C_3N_4 of TCN is between 2.82 eV ~ 3.19 eV. Thus the highest E_{VB} and E_{CB} potentials of the quantum g-C_3N_4 are 1.825 eV and −1.18 eV. Based on our previously reported band gap of TiO_2 (ca. 3.23 eV), the estimated E_{VB} and E_{CB} potentials of TiO_2 are 2.975 eV and −0.255 eV [33]. Obviously, the CB levels of both TiO_2 and quantum g-C_3N_4 were more negative than the reduction potential of $E^\circ(O_2/\cdot O_2^-)$ (-0.046 eV vs NHE), while only the h^+ on the VB of TiO_2 can react with OH^- or H_2O to generate ·OH because of the lower potential of $E^\circ(\cdot OH/H_2O)$ (2.68 eV vs NHE) and $E^\circ(\cdot OH/OH^-)$ (1.99 eV vs NHE) [44,45]. As discussed, the carriers' transfer between TiO_2 and g-C_3N_4 is facilitated for TCN. Thus the electrons on the CB of both TiO_2 and quantum g-C_3N_4 can react with O_2 to generate $\cdot O_2^-$, while only a small proportion of h^+ located on the VB of TiO_2 can generate ·OH. Consequently, both $\cdot O_2^-$ and h^+ are the main active species for TCN to photocatalytic degradation of tetracycline, while the ·OH

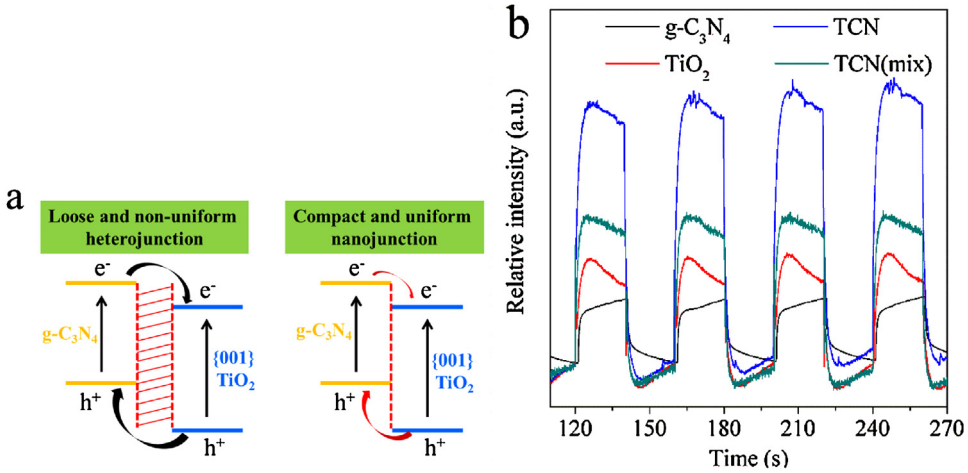

Fig. 8. (a) Proposed heterojunction differences between TCN and TCN(mix). (b) Transient photocurrents of TiO_2, TCN, TCN(mix), and g-C_3N_4 obtained in a 0.2 M Na_2SO_4 aqueous solution.

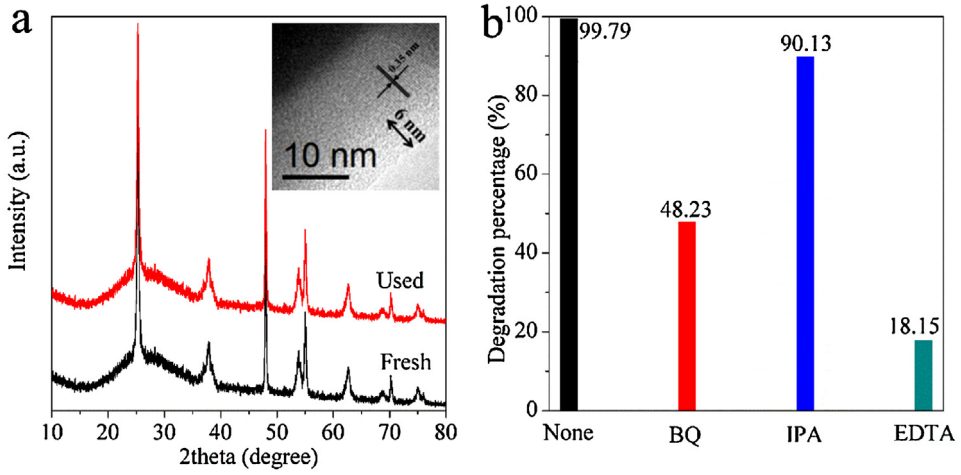

Fig. 9. (a) XRD patterns of TCN before and after the photocatalytic reaction. The TEM image (inset) of the used TCN confirms its structural stability. (b) Photocatalytic activities of TCN for the degradation of tetracycline in the presence of different scavengers under the xenon lamp irradiation.

has a negligible roleThis result also confirms the importance of tight contact between g-C_3N_4 quantum shell and TiO_2.

$$\text{Photocatalyst} + h\nu \rightarrow e^- + h^+ \quad (1)$$

$$e^- + O_2 \rightarrow \cdot O_2^- \rightarrow \cdot OH \quad (2)$$

$$h^+ + H_2O \rightarrow \cdot OH \quad (3)$$

$$\cdot OH/\cdot O_2^-/h^+ + \text{tetracycline} \rightarrow \text{degradationproduct} \quad (4)$$

4. Conclusions

In conclusion, we successfully prepared g-C_3N_4 quantum shell modified TiO_2 photocatalyst with an in situ formed core-shell quantum heterojunction for photocatalytic tetracycline degradation. The highest tetracycline degradation rate is 2.2 mg/min with the presence of 100 mg TCN photocatalyst under the xenon lamp irradiation, which is 2 times higher than that of TiO_2 and 2.3 times higher than that of bulk g-C_3N_4. It is believed that the uniform and compact contact interface, advantageous g-C_3N_4 quantum shell, richly available reaction sites, more surface adsorbed OH groups, and efficient electron transfer between TiO_2 and g-C_3N_4 quantum shell are key factors in determining the high photocatalytic activity of TCN photocatalyst. The present study demonstrates the significance of optimizing the contact interface structure of the heterojunction, which may inspire more ideas focusing on surface and interface engineering for efficient solar photocatalytic reaction systems.

Acknowledgements

This work was supported by the National Natural Science Foundation of China (No.51502143), Natural Science Foundation of Jiangsu Province (No.BK20150919), Key University Science Research Project of Jiangsu Province (No.15KJB430022), and the Startup Foundation for Introducing Talent of NUIST (2014r037).

Appendix A. Supplementary data

Supplementary data associated with this article can be found, in the online version, at http://dx.doi.org/10.1016/j.apcatb.2017.05.037.

References

[1] M. Yan, Y. Hua, F. Zhu, W. Gu, J. Jiang, H. Shen, W. Shi, Appl. Catal. B: Environ. 202 (2017) 518–527.
[2] M. Darwish, A. Mohammadi, N. Assi, J. Hazard. Mater. 320 (2016) 304–314.
[3] P. Huo, Z. Ye, H. Wang, Q. Guan, Y. Yan, J. Alloys Compd. 696 (2017) 701–710.
[4] H. Tong, S. Ouyang, Y. Bi, N. Umezawa, M. Oshikiri, J. Ye, Adv. Mater. 24 (2012) 229–251.

[5] X. Lang, X. Chen, J. Zhao, Chem. Soc. Rev. 43 (2014) 473–486.
[6] G. Liu, H.G. Yang, J. Pan, Y.Q. Yang, G.Q. Lu, H.M. Cheng, Chem. Rev. 114 (2014) 9559–9612.
[7] J.J. Chen, W.K. Wang, W.W. Li, D.N. Pei, H.Q. Yu, ACS Appl. Mater. Interfaces 7 (2015) 12671–12678.
[8] W. Guo, F. Zhang, C. Lin, Z.L. Wang, Adv. Mater. 24 (2012) 4761–4764.
[9] E.J. Crossland, N. Noel, V. Sivaram, T. Leijtens, J.A. Alexander-Webber, H.J. Snaith, Nature 495 (2013) 215–219.
[10] X. Wang, K. Maeda, A. Thomas, K. Takanabe, G. Xin, J.M. Carlsson, K. Domen, M. Antonietti, Nat. Mater. 8 (2009) 76–80.
[11] Y. Wang, X. Wang, M. Antonietti, Angew. Chem. 51 (2012) 68–89.
[12] K.S. Lakhi, D.-H. Park, K. Al-Bahily, W. Cha, B. Viswanathan, J.-H. Choy, A. Vinu, Chem. Soc. Rev. 46 (2017) 72–101.
[13] Y. Zheng, L. Lin, B. Wang, X. Wang, Angew. Chem. Int. Ed. 54 (2015) 12868–12884.
[14] M. Zhang, W. Jiang, D. Liu, J. Wang, Y. Liu, Y. Zhu, Y. Zhu, Appl. Catal. B: Environ. 183 (2016) 263–268.
[15] S. Wang, J. Lin, X. Wang, Phys. Chem. Chem. Phys. 16 (2014) 14656–14660.
[16] J. Qin, S. Wang, H. Ren, Y. Hou, X. Wang, Appl. Catal. B: Environ. 179 (2015) 1–8.
[17] J. Liu, Y. Liu, N.Y. Liu, Y.Z. Han, X. Zhang, H. Huang, Y. Lifshitz, S.T. Lee, J. Zhong, Z.H. Kang, Science 347 (2015) 970–974.
[18] L. Yao, D. Wei, Y. Ni, D. Yan, C. Hu, Nano Energy 26 (2016) 248–256.
[19] X. Li, G. Hartley, A.J. Ward, P.A. Young, A.F. Masters, T. Maschmeyer, J. Phys. Chem. C 119 (2015) 14938–14946.
[20] W.J. Ong, L.L. Tan, Y.H. Ng, S.T. Yong, S.P. Chai, Chem. Rev. 116 (2016) 7159–7329.
[21] D. Chen, K. Wang, W. Hong, R. Zong, W. Yao, Y. Zhu, Appl. Catal. B: Environ. 166–167 (2015) 366–373.
[22] S. Wang, W. Yao, J. Lin, Z. Ding, X. Wang, Angew. Chem. 53 (2014) 1034–1038.
[23] S. Wang, X. Wang, Angew. Chem. Int. Ed. 55 (2016) 2308–2320.
[24] Q. Han, B. Wang, J. Gao, Z. Cheng, Y. Zhao, Z. Zhang, L. Qu, ACS Nano 10 (2016) 2745–2751.
[25] Q. Liu, T. Chen, Y. Guo, Z. Zhang, X. Fang, Appl. Catal. B: Environ. 193 (2016) 248–258.
[26] J. Zhang, M. Zhang, C. Yang, X. Wang, Adv. Mater. 26 (2014) 4121–4126.
[27] H. Huang, S. Yang, R. Vajtai, X. Wang, P.M. Ajayan, Adv. Mater. 26 (2014) 5160–5165.
[28] S. Yang, Y. Gong, J. Zhang, L. Zhan, L. Ma, Z. Fang, R. Vajtai, X. Wang, P.M. Ajayan, Adv. Mater. 25 (2013) 2452–2456.
[29] X. Zhang, X. Xie, H. Wang, J. Zhang, B. Pan, Y. Xie, J. Am. Chem. Soc. 135 (2013) 18–21.
[30] P. Niu, L. Zhang, G. Liu, H.-M. Cheng, Adv. Funct. Mater. 22 (2012) 4763–4770.
[31] Z. Lu, L. Zeng, W. Song, Z. Qin, D. Zeng, C. Xie, Appl. Catal. B: Environ. 202 (2017) 489–499.
[32] K. Kočí, M. Reli, I. Troppová, M. Šihor, J. Kupková, P. Kustrowski, P. Praus, Appl. Surf. Sci. 396 (2017) 1685–1695.
[33] W. Wang, C. Lu, Y. Ni, Z. Xu, CrystEngComm 15 (2013) 2537.
[34] X. Song, Y. Hu, M. Zheng, C. Wei, Appl. Catal. B: Environ. 182 (2016) 587–597.
[35] T. Cai, Y. Liu, L. Wang, S. Zhang, Y. Zeng, J. Yuan, J. Ma, W. Dong, C. Liu, S. Luo, Appl. Catal. B: Environ. 208 (2017) 1–13.
[36] J. Li, B. Shen, Z. Hong, B. Lin, B. Gao, Y. Chen, Chem. Commun. 48 (2012) 12017–12019.
[37] J. Zhang, J. Xi, Z. Ji, J. Mater. Chem. 22 (2012) 17700.
[38] L. Ye, D. Wang, S. Chen, ACS Appl. Mater. Interfaces 8 (2016) 5280–5289.
[39] C. Ye, J.-X. Li, Z.-J. Li, X.-B. Li, X.-B. Fan, L.-P. Zhang, B. Chen, C.-H. Tung, L.-Z. Wu, ACS Catal. 5 (2015) 6973–6979.
[40] J. Wu, S. Yang, J. Li, Y. Yang, G. Wang, X. Bu, P. He, J. Sun, J. Yang, Y. Deng, G. Ding, X. Xie, Adv. Opt. Mater. 4 (2016) 2095–2101.
[41] H. Yu, R. Shi, Y. Zhao, G.I. Waterhouse, L.Z. Wu, C.H. Tung, T. Zhang, Adv. Mater. 28 (2016) 9454–9477.
[42] J. Xiao, Y. Xie, F. Nawaz, S. Jin, F. Duan, M. Li, H. Cao, Appl. Catal. B: Environ. 181 (2016) 420–428.
[43] Y.Y. Shang, X. Chen, W.W. Liu, P.F. Tan, H.Y. Chen, L.D. Wu, C. Ma, X. Xiong, J. Pan, Appl. Catal. B: Environ. 204 (2017) 78–88.
[44] R.R. Hao, G.H. Wang, H. Tang, L.L. Sun, C. Xu, D.Y. Han, Appl. Catal. B: Environ. 187 (2016) 47–58.
[45] S.G. Meng, X.F. Ning, T. Zhang, S.F. Chen, X.L. Fu, Phys. Chem. Chem. Phys. 17 (2015) 11577–11585.